Impact Insertion of Osteochondral Grafts: Interference Fit and Central Graft Reduction Affect Biomechanics and Cartilage Damage

Alvin W. Su,[1,2] Yunchan Chen,[1] Dustin H. Wailes,[1] Wong W. Van,[1] Shengqiang Cai,[2,3] Albert C. Chen,[1] William D. Bugbee,[4,5] Robert L. Sah[1,2,6]

[1]Department of Bioengineering, University of California-San Diego, La Jolla, California, [2]Program in Materials Science and Engineering, University of California-San Diego, La Jolla, California, [3]Department of Mechanical and Aerospace Engineering, University of California-San Diego, La Jolla, California, [4]Center for Musculoskeletal Research, Institute of Engineering in Medicine, University of California-San Diego, La Jolla, California, [5]Department of Orthopaedic Surgery, Scripps Clinic, La Jolla, California, [6]Department of Orthopaedic Surgery, University of California-San Diego, La Jolla, California

Received 7 March 2017; accepted 13 June 2017
Published online in Wiley Online Library (wileyonlinelibrary.com). DOI 10.1002/jor.23645

ABSTRACT: An osteochondral graft (OCG) is an effective treatment for articular cartilage and osteochondral defects. Impact of an OCG during insertion into the osteochondral recipient site (OCR) can cause chondrocyte death and matrix damage. The aim of the present study was to analyze the effects of graft-host interference fit and a modified OCG geometry on OCG insertion biomechanics and cartilage damage. The effects of interference fit (radius of OCG - radius of OCR), loose (0.00 mm), moderate (0.05 mm), tight (0.10 mm), and of a tight fit with OCG geometry modification (central region of decreased radius), were analyzed for OCG cylinders and OCR blocks from adult bovine knee joints with an instrumented drop tower apparatus. An increasingly tight (OCG - OCR) interference fit led to increased taps for insertion, peak axial force, graft cartilage axial compression, cumulative and total energy delivery to cartilage, lower time of peak axial force, lesser graft advancement during each tap, higher total crack length in the cartilage surface, and lower chondrocyte viability. The modified OCG, with reduction of diameter in the central area, altered the biomechanical insertion variables and biological consequences to be similar to those of the moderate interference fit scenario. Micro-computed tomography confirmed structural interference between the OCR bone and both the proximal and distal bone segments of the OCGs, with the central regions being slightly separated for the modified OCGs. These results clarify OCG insertion biomechanics and mechanobiology, and introduce a simple modification of OCGs that facilitates insertion with reduced energy while maintaining a structural interference fit. © 2017 Orthopaedic Research Society. Published by Wiley Periodicals, Inc. J Orthop Res

Keywords: articular cartilage; cartilage mechanics; impact mechanics; osteochondral autograft; osteochondral allograft

Repair with osteochondral graft (OCG) is one of the most effective surgical treatments for focal articular cartilage defects.[1,2] However, during insertion, impact loads are applied to the articular cartilage (AC) of the OCG and may result in chondrocyte death.[3] Viable chondrocytes and cartilage matrix integrity are important for clinical success of the surgery.[4,5] Typically, such OCG are prepared to be cylindrical, as are the osteochondral recipient (OCR) sites.

The biomechanics during the OCG insertion process reflect a series of impact events. The surgeon applies taps (N total) to insert the OCG into the OCR. For each tap (i), the peak force ($F_p{}^i$) increases as the OCG advances deeper.[6,7] $F_p{}^i$ increases substantially as the OCG is seated and bottoms out,[6,8] particularly for shorter OCGs that have relatively high structural stiffness.[9] The duration of each tap (T_i) is brief, ranging from 0.5 to 5 ms.[3,5,7,8] However, the distribution of the impact energy delivered to the graft, as well as the resultant cartilage compressive strain and extent of OCG advancement, have not been reported.

Understanding the mechanobiology of AC damage is important for preserving graft tissue health during surgery. Damage to the AC during OCG impact has been related to a variety of biomechanical factors. During OCG insertion, chondrocyte death has been associated with $F_p{}^i$.[6,8] For non-insertional impact scenarios, chondrocyte death has been associated with impact force,[8] contact stress,[10,11] compressive stress rate,[12,13] compressive strain,[10,14] compressive strain rate,[15] and total impact energy.[16–18] Articular cartilage failure has been described by fracture energy, or the energy normalized to crack area,[19] so that the parameter of energy input, or energy normalized to cartilage area, may provide an index related to cartilage damage.

The graft-host interference fit (radius of OCG - radius of OCR, ΔR) between OCG and OCR is one of the key parameters for surgical instrument design. Studies of analogous situations have assessed the effect of ΔR on insertion mechanics. Analogously, when nails are driven into wood, $F_p{}^i$ increases with nail diameter.[20] While a relatively tight fit can be beneficial to graft-host healing due to increased post-insertional graft stability, such a tight fit requires relatively high impact to achieve the insertion. The effect of ΔR on OCG insertion biomechanics and resultant cartilage damage remains to be elucidated.

The hypotheses of the present study were that during OCG insertion into OCR, (i) increasing tightness of graft-host interference fit leads to higher insertion energy and resultant AC damage, and (ii) a modified OCG geometry alters the mechanics of impact insertion and therefore reduces insertion energy and resultant AC damage. The specific aims were to

Grant sponsor: National Institutes of Health; Grant numbers: R01 AR055637, R01 AR044058, P01 AG007996; Grant sponsor: National Yang-Ming University; Grant number: n/a.
Correspondence to: Robert L. Sah, (T: 858-534-0821; F: 858-822-1614; E-mail: rsah@ucsd.edu)

determine the effects of ΔR for standard cylindrical OCG and OCR on (i) insertion biomechanics and (ii) damage to AC cells and tissue, and also (iii) to compare standard OCG and modified OCG for insertion biomechanics and the resultant AC damage.

MATERIALS AND METHODS

Study Design

Study 1

The effects of ΔR on biomechanics of insertion and damage to articular cartilage were assessed in terms of the total number of taps (N), cumulative energy density delivered to cartilage of OCG ($\Sigma W_{S,i}^{OCG}$), and viability of chondrocytes at the articular surface ($V^{AC,OCG}$), as well as the relationship between cumulative OCG advancement ($u_{adv}[m]$) and energy delivered ($W^{Tamp}[m]$) after the m^{th} tap for standard cylindrical OCG and OCR with three study groups: (i) loose fit, $\Delta R = 0.00$ mm ($n = 7$), (ii) moderate fit, $\Delta R = 0.05$ mm ($n = 6$), and (iii) tight fit, $\Delta R = 0.10$ mm ($n = 6$).

Study 2

The effect of OCG geometry on insertion biomechanics and articular cartilage damage was assessed by comparing the last group in Study 1 to an additional group, also with original $\Delta R = 0.10$ mm, but with modified OCG geometry as described below to have a reduced ΔR in a central region ($n = 7$).

Detailed Experimental Methods

Sample Preparation

A total of 41 OCGs and 26 OCRs were prepared from the distal femora of six adult bovine knees, obtained fresh from an abattoir within 24 h of sacrifice and using sterile technique. With a coring bit and diamond-edged saw, OCGs were prepared to a radius of 2.40 mm and to a subchondral bone height of 5.00 mm. The OCRs were prepared as osteochondral cuboid blocks with a base of $\sim 15 \times 15\,mm^2$, and height of $\sim$15 mm. Of the 41 OCGs, 15 served as control samples without any impact loading treatment. In Study 1, 19 OCGs were used. In Study 2, seven OCGs were prepared to a modified geometry. During OCG and OCR preparation, all samples were kept moist and cool by irrigation with phosphate buffered saline (PBS).

Graft-Host Interference Fit (ΔR)

Graft-host interference fit *(ΔR)* was calculated as the radius of the OCG (2.40 mm) minus the radius of the OCR (a^{OCR}). The recipient sites were drilled in the center of the cuboid blocks to a depth of 10 mm from the articular surface using stainless steel drill bits of 4.80, 4.70, and 4.60 mm in diameter. Therefore, a^{OCR} values were 2.40, 2.35, and 2.30 mm, respectively, and the resulting three levels of ΔR were 0.00, 0.05, and 0.10 mm (Fig. 1A and C).

OCG With Modified Geometry

Starting from the standard OCG, a central region with decreased radius was created. Specifically, a $\sim$0.25 mm reduction in radius was created in a 2 mm long (deep) region, extending down from 1.5 mm below the cartilage-bone junction (Fig. 1B). This was achieved by holding the OCG in a collet (diameter 4.8 mm) of a mill machine, and then gradually translating a 2 mm-thick rectangular hand file, mounted on the platform of the drill mill, for 0.25 mm after initial contact. During this process, the sample was irrigated with PBS to cool and hydrate the tissue. In addition, care was taken to not disturb the articular surface.

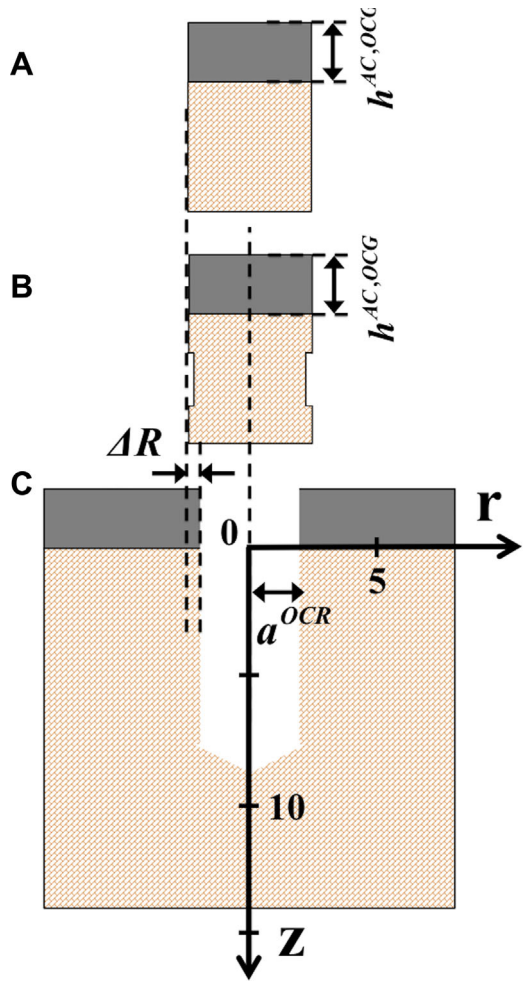

Figure 1. Schematic of geometries of OCG and OCR. (A) standard OCG, (B) modified OCG, and (C) OCR. Indicated is graft-host interference fit (ΔR).

OCG Insertion

Standard and modified OCG were inserted in a standardized way, applying a prescribed energy density, $W_{S,i}^{PE}$, for each tap i and recording the resultant impact load, $F_i(t)$, the movement of the cartilage surface, $u_i^{Tamp}(t)$, and the OCG advancement distance with each tap, $u_{adv}{}^i$. The OCG was pre-inserted manually, past the AC, seating it at the bone, $\sim$1.5 mm into the OCR. A rigid tamp was then placed atop the AC surface. Serial taps were applied to the OCG via the rigid tamp, using a drop tower apparatus instrumented with a load sensor at the impaction surface, providing $F_i(t)$, and a laser displacement sensor assessing the position of the articular surface of the OCG via the tamp, providing $u_i^{Tamp}(t)$. After each tap, a side-view digital photograph (0.02 mm pixel resolution) was taken to allow measurement of the cumulative OCG advancement distance after tap i, $u_{adv}[m]$, and from these, the incremental OCG advancement distance, $u_{adv}{}^i$, for each tap. The applied energy density, energy/OCG cartilage area, of each tap i, $W_{S,i}^{PE}$, was set by using a weight at various heights (with potential energy that is the product of mass, acceleration due to gravity, and height) from the OCG bone surface. The first tap had $W_{S,1}^{PE}$

of 0.9 mJ/mm^2. Successive taps had energy density increasing by a factor of 1.5, so that $W_{S,i}^{PE} = 0.9 \times 1.5^{(i-1)}$ mJ/mm^2. Successive taps were applied until tap N, after which the articular surface of the OCG was flush with that of the OCR (Fig. 2A).

Chondrocyte Viability Analysis

After the final impact, the articular cartilage was analyzed for percentage of viable chondrocytes.[3,21] The articular cartilage of the OCG was sliced off as a disc with a sterile scalpel and incubated for 24 h in medium with 10% FBS. The disc was then stained with LIVE/DEAD® (Thermo Fisher Scientific, Waltham, MA) as previously described,[21] imaged *en face* with fluorescence microscopy in the central (3.75 × 0.75 mm) area, spanning most of the sample. Image processing was performed to determine viability, $V^{AC,OCG}$, as live cells / (live cells + dead cells).

Articular Cartilage Surface Analysis

Finally, matrix damage was assessed by determining L_{crack}, the total length of cracks at the articular surface. Samples were stained with India Ink and photographed.[22] Using NIH ImageJ software, both edges of each crack were traced, and the total edge lengths were summed. L_{crack} was taken as half of the total edge length. The total surface crack length of each OCG was determined as the average of measurements by three independent observers. The measurement was highly reproducible, with intra-observer correlation coefficient of 0.98.

Micro-Computed Tomography (μCT) Imaging

One sample of each experimental group was chosen for μCT scanning for qualitative assessment of the top, middle and bottom parts of graft-host subchondral bone interface. The μCT scan settings were those described previously with (9 μm)^3 voxel resolution.[4]

Biomechanics Calculations

All biomechanical variables and parameters are listed in Table 1. Mechanical variables were quantified from $F_p^i(t)$, $u_i^{AC,OCG}$(t), and u_{adv}^i. Peak contact stress (σ_p^i) was calculated as the peak contact force (F_p^i) normalized to the surface area of the OCG (A^{OCG}, 18.09 mm^2). Impact impulse (I_C^i) was quantified by integrating impact force over time for the duration (T_i) of the impact. Peak axial displacement of AC of OCG ($u_{p,i}^{AC,OCG}$) was taken as peak axial displacement of the tamp ($u_{p,i}^{Tamp}$) minus the OCG advancement distance during for each tap (u_{adv}^i). Peak axial strain of the AC of OCG, ε_p^i, was calculated by normalizing $u_{p,i}^{AC,OCG}$ to the AC thickness of the OCG ($h^{AC,OCG}$). For each tap i, the energy delivered by the tamp to the sample, W_i^{Tamp}, was calculated by integrating $F_i(t)$ over the axial displacement of the tamp, $u_i^{Tamp}(t)$. Energy delivered to the AC of the OCG, W_i^{OCG} and to advancing the OCG into OCR, W_i^{adv}, were determined by an energy balance. For each tap, i, W_i^{Tamp} was assumed to be divided into W_i^{OCG} and the work to advance the OCG into the OCR, and accordingly apportioned to the cartilage by the peak deformation of AC of OCG relative to the movement of bone, with $W_i^{OCG} = W_i^{Tamp} \bullet (u_{p,i}^{AC,OCG} / u_{p,i}^{Tamp})$, and $W_i^{adv} = W_i^{Tamp} \bullet (u_{adv}^i / u_{p,i}^{Tamp})$ (Fig. 2A). The corresponding energy density delivered to the AC of an OCG by tap i, $W_{S,i}^{OCG}$, was calculated by normalizing W_i^{OCG} to A^{OCG}. The energy density delivered to the bone interface for OCG advancement into OCR, $W_{S,i}^{adv}$, was calculated by normalizing W_i^{adv} to the increment in host-graft bone interface area, A_{adv}^i, encompassing the OCG travel distance u_{adv}^i, so that $A_{adv}^i = \pi \times 4.80\,\text{mm} \times u_{adv}^i$. Cumulative energy delivered to OCG samples through tap m, $W_{Tamp}[m]$, was calculated as $\Sigma_{i=1}^{m} W_i^{\text{Tamp}}$. Cumulative energy density delivered to the articular

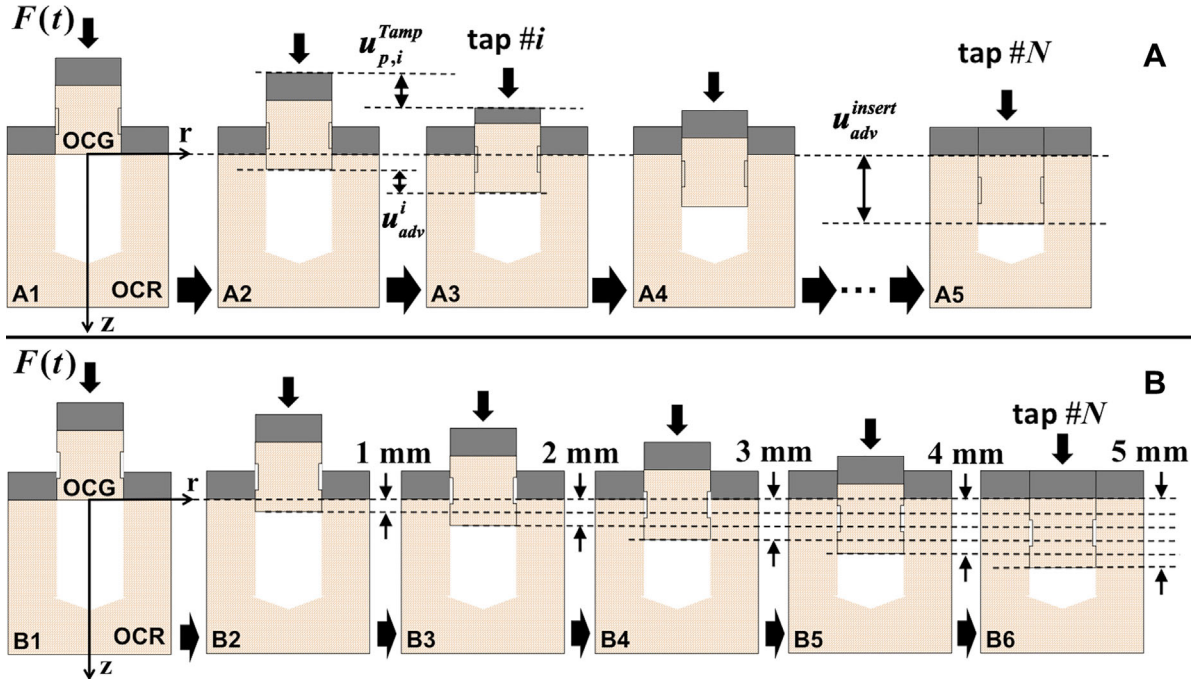

Figure 2. Schematic of impact insertion of OCG as well as mechanical variables and parameters. (A) Advancement of OCG into OCR, from starting position (A1), advancing with successive taps (A2–5), to final flush position (A5). Tap #, i, out of N total taps. Peak tamp advancement with tap i, $u_{p,i}^{Tamp}$. OCG (bone base) advancement with tap i, u_{adv}^i, and overall advancement at full insertion, u_{adv}^{insert}. (B) OCG at five successive insertion positions, at insertion depths of 1–5 mm (B2-B6), at which parameters were estimated.

Table 1. Biomechanical Parameters and Variables

Parameter	Definition	Unit
A^{OCG}	Articular cartilage surface area of OCG	mm2
a^{OCR}	Radius of OCR	mm
$h^{AC,OCG}$	Thickness of AC of OCG prior to impact	mm
i	Sequential tap number to impact insert OCG into OCR, $i = 1,2,\ldots,N$	–
${W_{S,i}}^{PE}$	Applied energy density for tap #i	mJ/mm^2
j	Section region, into which cylindrical insertion area is divided for analysis, with j=i, ii, ..., v	–
m	Tap number, up to which impact insertion of OCG into OCR is evaluated, for $m = 1, 2, ..., N$	–

Variable	Definition	Unit
${A_{adv}}^{i}$	Increment in host-graft bone interface area between OCG and OCR during tap #i	mm^2
$F(t)$	Contact force applied by the tamp	N
${F_p}^{i}$	Peak force applied by the tamp during tap #i	N
${I_c}^{i}$	Impact impulse of the impact event of tap #i	N•ms
L_{crack}	Total crack lengths on articular cartilage surface of OCG	mm
N	Last tap number for insertion sequence	–
T_i	Impact time duration during tap #i	ms
t	Relative time for impact event	ms
${u_{adv}}^{i}$	OCG advancement distance during tap #i	mm
${u_{adv}}^{insert}$	Overall advancement with full insertion	mm
$u_{adv}[m]$	Cumulative OCG advancement distance after tap #m	mm
${u_i}^{Tamp}(t)$	Axial displacement of the tamp during tap #i	mm
${u_{p,i}}^{AC,OCG}$	Peak axial compressive displacement of AC of OCG during tap #i	mm
${u_{p,i}}^{Tamp}$	Peak axial displacement of the tamp during tap #i	mm
$V^{AC,OCG}$	Surface chondrocyte viability of AC of OCG after insertion	%
W_i^{adv}	Energy advancing OCG into OCR during tap #i	mJ
$W_{insert}^{AC,OCG}$	Total cumulative energy delivered to AC of OCG by the completion of insertion	mJ
W_i^{OCG}	Energy delivered to AC of OCG during tap #i	mJ
W_i^{Tamp}	Energy delivered by the tamp to the sample during tap #i	mJ
$W^{Tamp}[m]$	Cumulative energy delivered by the tamp to the sample after tap #m	mJ
${W_{S,i}}^{OCG}$	Energy density delivered to AC of OCG during tap #i	mJ/mm^2
${W_{S,m}}^{OCG}$	Cumulative energy density delivered to AC of OCG after tap #m	mJ/mm^2
${W_{S,j}}^{adv}$	Sectional energy density of OCG advancement for section #j	mJ/mm^2
${\varepsilon_p}^{i}$	Peak axial strain of AC of OCG during tap #i	mm/mm
$\Sigma {W_{S,N}}^{OCG}$	Total cumulative energy density delivered to AC of OCG by the completion of insertion	mJ/mm^2
${\sigma_p}^{i}$	Peak contact stress during tap #i	MPa

cartilage through tap m, $W_{S,m}^{OCG}$, was calculated as $\Sigma_{i=1}^{m} W_{S,i}^{OCG}$. With the completion of insertion (when $m = N$), this summation is the total cumulative energy density delivered to the AC of the OCG, $W_{insert}^{AC,OCG}$.

In Study 2, the energy associated with each 1 mm of OCG travel into the OCR was calculated to allow overall assessment of the tapered geometry, since the OCG samples advanced to a different extent during the successive taps. To do so, analysis was performed for advancement in five sequential 1 mm sections, j = i, ii, …, v, with the first portion starting at 0 in the z axis. Thus, for each section, the graft-host interface area was 15.08 mm^2 (Fig. 2B). The sectional energy density of OCG advancement (${W_{S,j}}^{adv}$) was calculated as the sum of weighted W_i^{adv} values for each section j, partitioning the W_i^{adv} of each tap according to the OCG travel distance within each section. For example, if during tap #m, the OCG advanced 1.5 mm, through the final 0.2 mm in section #ii, all the way (1.0 mm) through section #iii and then into the beginning 0.3 mm into section #iv, then $(0.2/1.5){W_m}^{adv}$ was taken to contribute to ${W_{S,ii}}^{adv}$, and $(0.3/1.5){W_m}^{adv}$ to ${W_{S,iv}}^{adv}$, with ${W_{S,iii}}^{adv} = (1.0/1.5){W_m}^{adv}$.

Statistical Analysis

The effects of ΔR (0.00, 0.05, 0.10 mm, and 0.10 mm with modified OCG geometry) on $\Sigma {W_{S,i}}^{OCG}$, N, $V^{AC,OCG}$ and L_{crack} were assessed using one-way ANOVA with Tukey post-hoc test. The effects of ΔR on ${F_p}^{i}$, ${\sigma_p}^{i}$, ${I_C}^{i}$, T_i, ${u_{p,i}}^{Tamp}$, ${u_{p,i}}^{AC,OCG}$, ${u_{adv}}^{i}$, ${\varepsilon_p}^{i}$, ${W_{S,i}}^{Tamp}$, ${W_{S,i}}^{OCG}$, ${W_{S,i}}^{adv}$ were assessed using one-way ANOVA for the first eight taps ($1 \le i \le 8$) where data were recorded for more than two groups, and unpaired two-tailed student t-test for $9 \le i \le 10$ where data were from the two groups with tight fit ($\Delta R = 0.10$ mm, with vs. without modified OCG geometry). In addition, the effect of OCG geometry modification, which was $\Delta R = 0.10$ mm, with vs. without modified OCG geometry, on ${W_{S,j}}^{adv}$ of each section #j, were assessed using unpaired two-tailed student t-test. The relationship between L_{crack} and $W_{insert}^{AC,OCG}$, $\Sigma {W_{S,N}}^{OCG}$ for all OCG samples in both studies was assessed by linear

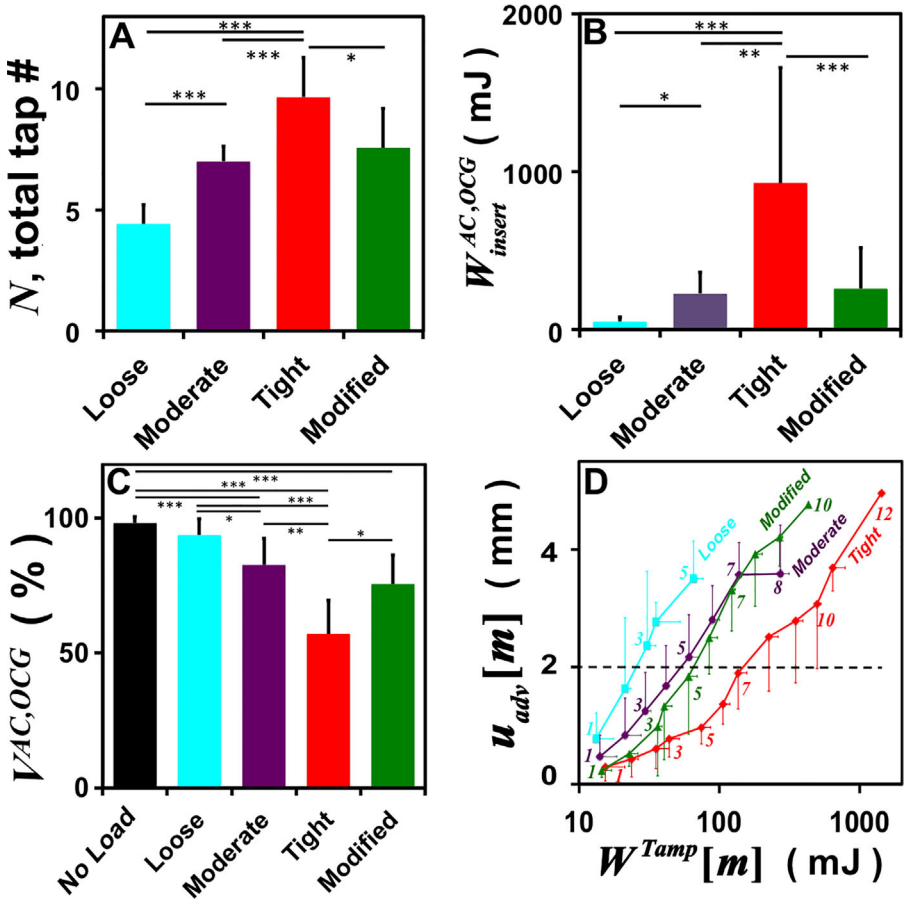

Figure 3. Effects of interference fit (ΔR) and OCG geometry modification on insertion mechanics. (A) Total number of taps (N). (B) Total energy delivered to AC of OCG by the completion of insertion ($W_{insert}^{AC,OCG}$). (C) Viability of surface chondrocytes ($V^{AC,OCG}$). (D) Cumulative OCG advancement ($u_{adv}[m]$) as a function of cumulative insertion energy ($W^{Tamp}[m]$), after each tap, i, as labeled.

regression. Data are expressed as mean ± SD. Significance was set at $\alpha = 0.05$.

RESULTS

Study 1

Tighter interference fit resulted in more total tap numbers and higher cumulative energy delivered to the AC of the OCG by the completion of insertion (Fig. 3A–B). Compared to the loose fit group, $\Delta R = 0.00$ mm, the tight fit group, $\Delta R = 0.10$ mm, required two times more taps (4.4 vs. 9.7, Fig. 3A) and 25 times higher $W_{insert}^{AC,OCG}$ (53 mJ vs. 927 mJ, Fig. 3B) and thus higher $\Sigma W_{S,N}{}^{OCG}$. When looking at $u_{adv}[m]$ as a function of $\log(W^{Tamp}[m])$, tighter interference fit presented a "right-shift" phenomenon of the sigmoid curve (Fig. 3D). This indicated that more energy was delivered to reach the same level of OCG advancement into the OCR.

During the initial insertion taps, tighter interference fit led to higher $F_p{}^i$, $\sigma_p{}^i$ (taps #1-3), $W_{S,i}{}^{OCG}$ (taps #2-4), and $W_{S,i}{}^{adv}$ (tap #2), as well as shorter T_i (tap #1, 3, 4) and lower $u_{adv}{}^i$ (tap #1, 2, 4). $W_{S,i}{}^{Tamp}$, $u_{p,i}{}^{AC,OCG}$, $I_C{}^i$, and $\varepsilon_p{}^i$ were generally similar among loose, moderate, and tight fit groups (Fig. 4A–C, Table S-1).

Tighter interference fit resulted in more surface chondrocyte death and cartilage tissue cracks in the OCG (Figs. 3C and 4D–F). The mean values of $V^{AC,OCG}$ were 98%, 94%, 83%, 57% for no load control, loose, moderate, and tight fit groups, respectively.

Study 2

Modification of OCG geometry resulted in fewer total tap numbers and lower $W_{insert}^{AC,OCG}$, cumulative energy delivered to AC of OCG, by the completion of insertion (Fig. 3A and B). The mean value of N decreased from 9.7 to 7.6, and $\Sigma W_{S,i}{}^{OCG}$ decreased 72%. When considering $u_{adv}[m]$ as a function of $W^{Tamp}[m]$ (on a log scale), OCG geometry modification led to a "left-shift" of the sigmoidal curve (Fig. 3D).

At the middle part of insertion, modified OCG geometry led to lower $W_{S,i}{}^{OCG}$ (taps #4–6) as well as higher $u_{p,i}{}^{Tamp}$, and $u_{adv}{}^i$ (tap #6 for both). The other mechanical variables were generally similar (Fig. 4A–C, Table S-1).

Surface chondrocyte death and cartilage tissue cracks were less among modified OCG (Fig. 3C and 4D–F). The mean value of $V^{AC,OCG}$ for modified OCG was 76% compared to 57% for non-modified OCG.

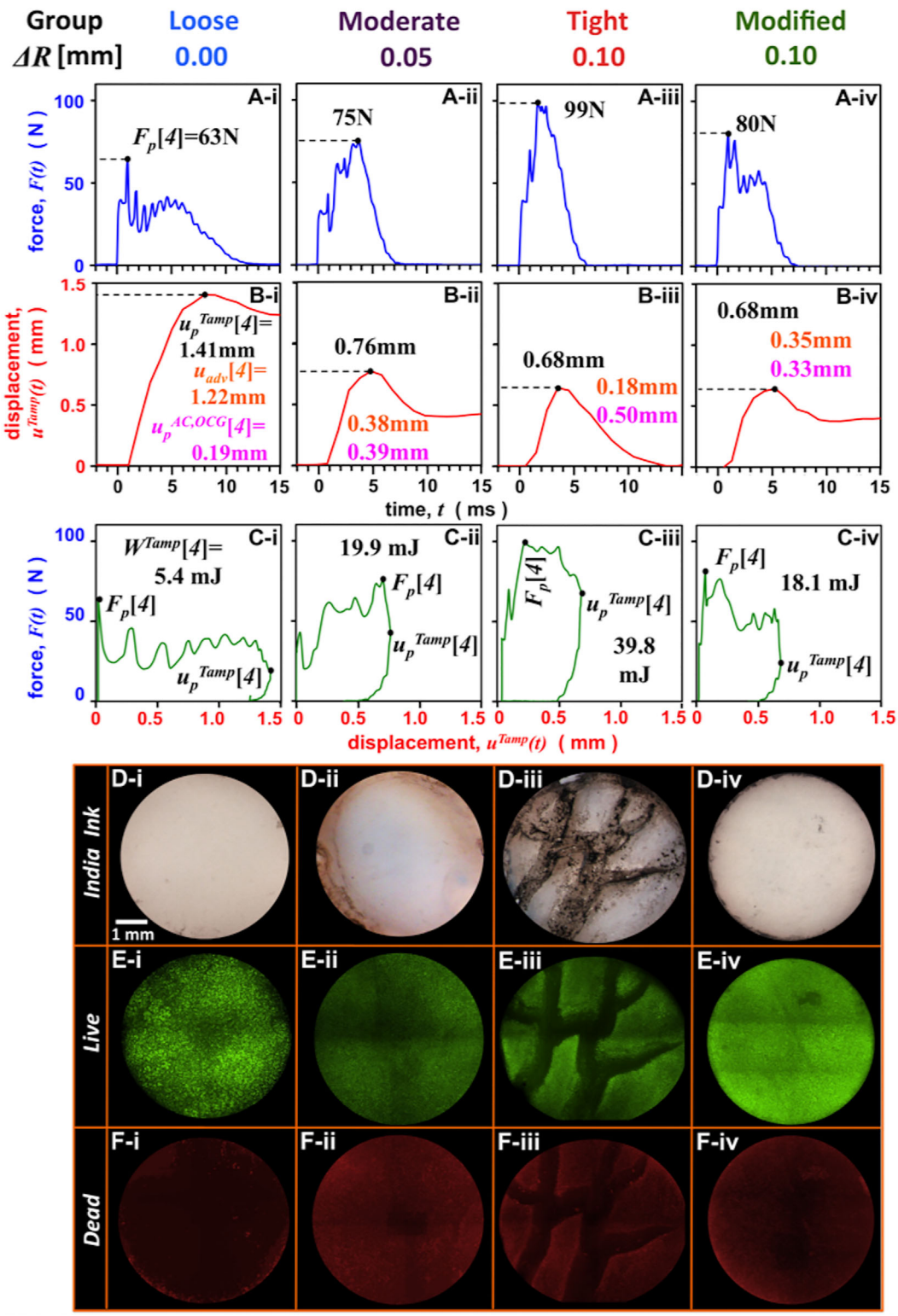

Figure 4. Typical effects of interference fit (ΔR) and OCG geometry modification on impact mechanics and cartilage damage. (i-iv) Study Groups are standard OCG geometry with OCR that generate (i) loose, (ii) moderate, and (iii) tight interference fits, and (iv) modified OCG geometry into OCR with tight fit. (A-C) Mechanics of OCG insertion. For 4th tap, time courses of measured (A) tamp contact force, (B) tamp displacement and (C) parametric plot of tamp contact force and displacement, illustrating energy-associated loop. In (B) are indicated peak tamp advancement increment, divided amongst OCG advancement, $u_{adv}[4]$, and deduced cartilage compaction, $u_p^{AC,OCG}[4]$. In (C) are indicated delivered energy values. (D–F) *En face* microscopic analysis of effects on cartilage. (D) Reflected light view of articular surface after India Ink staining, showing cartilage damage and cracks. Fluorescence view of articular surface after Live-Dead fluorescence staining, with (E) live cell indicator in green, and (F) dead cell indicator in red.

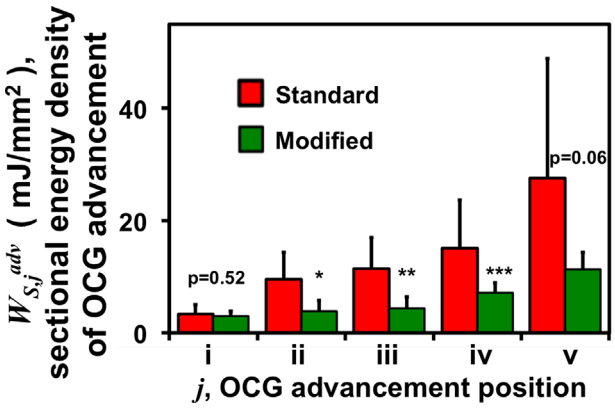

Figure 5. Effect of OCG geometry modification on energy for OCG advancement to defined depths. Data of cumulative energy density after individual taps was interpolated to estimate values at the indicated positions of five sections (i-v) of 1 mm in depth, each encompassing the 0–5 mm insertion depth.

OCG geometry modification resulted in less sectional energy density of OCG advancement in the middle part of insertion. Modified OCGs had lower $W_{S,ii}^{adv}$, $W_{S,iii}^{adv}$, $W_{S,iv}^{adv}$ compared to non-modified OCGs. $W_{S,i}^{adv}$, $W_{S,v}^{adv}$ were not different between the two groups ($p = 0.52$ and 0.06, respectively), but the mean value of $W_{S,v}^{adv}$ was lower for modified OCG (Fig. 5).

L_{crack} was strongly correlated with $W_{insert}^{AC,OCG}$ and therefore $\Sigma W_{S,N}^{OCG}$ ($R^2 = 0.93$, $p < 0.0001$, Fig. 6). The mean value of L_{crack} of tight fit group was 11.58 mm, ~100-fold that (0.11 mm) of the loose fit group, and ~6-fold that (2.04 mm) with OCG geometry modification.

Qualitatively, μCT showed differences in interference fit (Fig. 7). The tight fit sample presented the

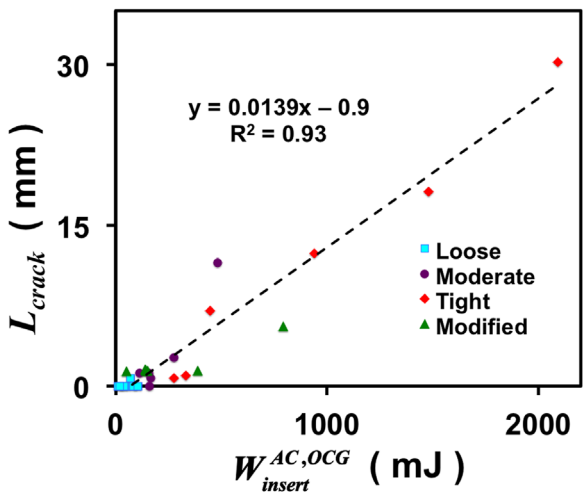

Figure 6. Correlation analysis of total crack length on graft cartilage surface (L_{crack}) with total energy delivered to AC of OCG by the completion of insertion ($W_{insert}^{AC,OCG}$). Data for all samples, with loose, moderate, and tight interference fits of standard samples, and also tight interference fit of modified samples are indicated with colored symbols.

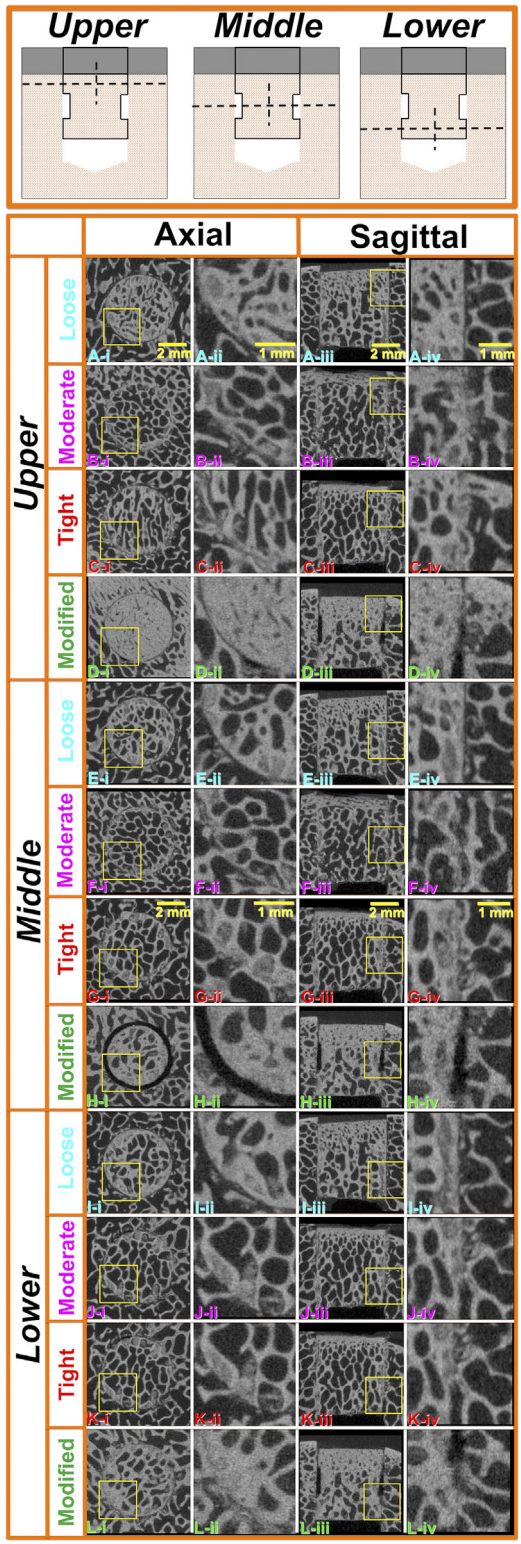

Figure 7. Qualitative μCT assessment of subchondral bone compaction at graft-host interface after OCG insertion. (A–L) μCT image slices were selected from (A–D) Upper, (E-H) Middle and (I–L) Lower portion of the graft-host subchondral bone interface, in (i-ii) Axial and (iii-iv) Sagittal orientations. Study Groups are standard OCG geometry with OCR that generate (A, E, I) Loose, (B, F, J) Moderate, and (C, G, K) Tight interference fits, and (D, H, L) Modified OCG geometry into OCR with tight fit. Yellow light box in (i) and (iii) indicates the zoom-in area of interest in (ii) and (iv), respectively.

most apparent subchondral bone compaction at the graft-host interface. In the loose fit sample, some empty space (devoid of bone) was visible at the graft-host interface. Such space was less for the moderate fit sample, and least for the tight fit sample. The modified OCG sample exhibited a clearly visible space without subchondral bone contact at the offset middle part of the graft, and patterns similar to the non-modified sample at top and bottom of the graft.

DISCUSSION

The present study indicates that small variations in graft-host interference fit can markedly affect the biomechanics of OCG insertion and the resultant health of, or extent of damage to, the articular cartilage. Tighter (OCG - OCR) fit resulted in more taps and more insertion energy for insertion as well as more cell death. With the same graft-host fit, modification of the OCG subchondral bone geometry to reduce the interference in the central part of the graft, leaving the proximal and distal region with the same interference fit, reduced the insertional energy and subsequent damage to the articular cartilage. These results thus provide important considerations about the graft-host interference fit for design of surgical methods and instruments that achieve impact insertion of osteochondral grafts, while preserving the health of the grafted articular cartilage.

The design of the present study involved a number of tradeoffs. Osteochondral tissue from the adult bovine distal femur was used as a model system, providing mature articular cartilage that is consistently healthy although different from human articular cartilage. Compared to human articular cartilage in the distal femur, bovine articular cartilage is thinner ($h^{AC,OCG}$ of 1.5 mm in the present study versus 2.2–2.5 mm in human[23,24]); both human and bovine cartilage exhibit a range of depth-varying compressive moduli and stiffness depending on geometry and loading condition (e.g., 0.3–49 MPa[25,26] and 3.1–13.0 MPa[27–29]). The subchondral bone of adult bovines can be as high as 10 GPa,[30] markedly higher than that of ~1 GPa, of humans.[31] In addition, the OCG were small in diameter compared to those used clinically (diameter of OCG autografts typically up to 10.0 mm and of OCG allografts that could be 15.0 mm or more.[32,33]) in order to generate reasonable numbers of samples for statistical purposes. In addition, the ΔR can have a range of values for different instrumentation systems. In the present study, the diameter of OCGs was 4.8 mm, and the largest ΔR was 0.1 mm. The present study utilized bovine tissue to validate the experimental methodologies and address the scientific questions and practical problems of OCG insertion. Also, the strong correlation of $W_{insert}^{AC,OCG}$ and $\Sigma {W_{S,N}}^{OCG}$ with cartilage tissue damage may be translated to different sizes of osteochondral samples.[34]

In addition, at completion of insertion, a gap was left between the base of OCG and the bottom of the OCR to facilitate biomechanical analysis. Such a gap is not typical in clinical practice but allowed the experimental design of the present study to focus on the process of graft advancement into the recipient site. In certain practical scenarios (if the graft is "proud"), impact load might be applied, even when the base of the OCG is in contact with the bottom of the OCR, in order to "bottom out" the graft. This issue was not addressed in the present study, as such loading is associated with high insertional loads and cell death.[8]

There are a variety of graft-host interface interactions that likely account for the higher insertion energy required for tight fit samples. During each tap, the applied impact energy was partitioned to two major components: the AC of OCG, and the OCG-OCR subchondral bone system. Using a simplified model of two structures connected in series, mechanical analyses indicated that more energy is partitioned into the component with the lower stiffness. As the OCG advances further into the OCR, the subchondral bones of both can undergo elastic and plastic deformations, as well as trabecular fracture at the contact interface. The magnitude of the above increases with increasing graft-host interference fit, thus resulting in a higher equivalent stiffness. Therefore, with the same ${W_{S,i}}^{PE}$, higher ΔR led to higher ${W_{S,i}}^{OCG}$ and less ${u_{adv}}^{i}$. Consequently, the tight fit group required more taps with higher $\Sigma {W_{S,i}}^{OCG}$ to complete the insertion, and resulted in more damage to the articular cartilage.

The modification of OCG geometry decreased the equivalent stiffness of the graft-bone subchondral bone system by reducing the graft-host interface contact area. This was indicated by the lower ${W_{S,j}}^{adv}$ in the modified OCG group when the OCG subchondral bone advanced into the OCR ($j =$ ii to iv). Clinically, from the perspective of bone fracture fixation, osseous healing can occur with a small gap even with slight graft-host relative motion. [35]

The effects of ΔR and OCG geometry modification on graft stability after insertion have yet to be elucidated. Graft stability may be modulated by graft length and diameter, as well as repeated insertion, as quantified by the pull-out load.[36] However, *in vivo* after surgery, the OCG and OCR sustain repetitive compressive and shear loads, so that a variety of mechanical indices of stability are of interest. While the results of the present study indicate that lower ΔR facilitates OCG insertion with less impact energy, such ΔR may also predispose an OCG to excessive micro-motion and loosening.

In conclusion, the present study provided new information about the effect of graft-host interference fit on OCG insertion biomechanics and its biological consequences. The optimal graft-host interference fit thus depends upon the delicate balance between preserving graft cartilage health and adequate post-insertional graft stability. Based on the foundations of these findings, further investigation can be carried out toward clinical translation. The OCG geometry

modification may improve this balance, mitigating injury to graft cartilage while restricting lateral motion with a relatively larger ΔR and tighter fit at proximal and distal portions of the graft. Investigation of other OCG-OCR heights and ΔR would be useful to further characterize the geometry modification.

AUTHORS' CONTRIBUTION

All authors were significantly involved in study design, execution of experiments, data analysis and manuscript preparation. All authors concur with the content and approved the final submission of the present manuscript.

ACKNOWLEDGMENTS

Funding was from NIH RO1 AR055637 (WDB), NIH R01 AR044058 (RLS), NIH PO1 AG07996 (RLS). National Yang-Ming University, Taiwan (AWS). Potential Conflicts of Interest are the following. Board Membership: Orthopaedic Research Society (RLS); Consultancy: Joint Restoration Foundation (WDB). Stock or Stock Options. GlaxoSmithKline (RLS), Johnson and Johnson (RLS), Medtronic (RLS), Moximed (WDB), OrthAlign (WDB). Consultancy: Joint Restoration Foundation (WDB), a nonprofit tissue bank and distributor of osteochondral allografts, DePuy (WDB), Organogenesis (WDB), OrthAlign (WDB). Intellectual Property Royalties: DePuy (WDB), Smith & Nephew (WDB), Zimmer Biologics (WDB).

REFERENCES

1. Hangody L, Vasarhelyi G, Hangody LR, et al. 2008. Autologous osteochondral grafting-technique and long-term results. Injury 39:S32–S39.
2. Cole BJ, Pascual-Garrido C, Grumet RC. 2009. Surgical management of articular cartilage defects in the knee. J Bone Joint Surg Am 91:1778–1790.
3. Borazjani BH, Chen AC, Bae WC, et al. 2006. Effect of impact on chondrocyte viability during the insertion of human osteochondral grafts. J Bone Joint Surg Am 88:1934–1943.
4. Pallante-Kichura AL, Cory E, Bugbee WD, et al. 2013. Bone cysts after osteochondral allograft repair of cartilage defects in goats suggest abnormal interaction between subchondral bone and overlying synovial joint tissues. Bone 57:259–268.
5. Pallante AL, Chen AC, Ball ST, et al. 2012. The in vivo performance of osteochondral allografts in the goat is diminished with extended storage and decreased cartilage cellularity. Am J Sports Med 40:1814–1823.
6. Whiteside RA, Jakob RP, Wyss UP, et al. 2005. Impact loading of articular cartilage during transplantation of osteochondral autograft. J Bone Joint Surg Br 87:1285–1291.
7. Pylawka TK, Wimmer M, Cole BJ, et al. 2007. Impaction affects cell viability in osteochondral tissues during transplantation. J Knee Surg 20:105–110.
8. Patil S, Butcher W, D'Lima DD, et al. 2008. Effect of osteochondral graft insertion forces on chondrocyte viability. Am J Sports Med 36:1726–1732.
9. Kock NB, van Susante JL, Wymenga AB, et al. 2006. Press-fit stability of an osteochondral autograft: influence of different plug length and perfect depth alignment. Acta Orthop 77:422–428.
10. Repo RU, Finlay JB. 1977. Survival of articular cartilage after controlled impact. J Bone Joint Surg Am 59-A:1068–1076.
11. Torzilli PA, Grigiene R, Borrelli J Jr., et al. 1999. Effect of impact load on articular cartilage: cell metabolism and viability, and matrix water content. J Biomech Eng 121:433–441.
12. Ewers BJ, Dvoracek-Driksna D, Orth MW, et al. 2001. The extent of matrix damage and chondrocyte death in mechanically traumatized articular cartilage explants depends on rate of loading. J Orthop Res 19:779–784.
13. Milentijevic D, Torzilli PA. 2005. Influence of stress rate on water loss, matrix deformation and chondrocyte viability in impacted articular cartilage. J Biomech 38:493–502.
14. Torzilli PA, Deng XH, Ramcharan M. 2006. Effect of compressive strain on cell viability in statically loaded articular cartilage. Biomech Model Mechanobiol 5:123–132.
15. Quinn TM, Allen RG, Schalet BJ, et al. 2001. Matrix and cell injury due to sub-impact loading of adult bovine articular cartilage explants: effects of strain rate and peak stress. J Orthop Res 19:242–249.
16. Szczodry M, Coyle CH, Kramer SJ, et al. 2009. Progressive chondrocyte death after impact injury indicates a need for chondroprotective therapy. Am J Sports Med 37:2318–2322.
17. Finlay JB, Repo RU. 1979. Energy absorbing ability of articular cartilage during impact. Med Biol Eng Comput 17:397–403.
18. Burgin LV, Aspden RM. 2008. Impact testing to determine the mechanical properties of articular cartilage in isolation and on bone. J Mater Sci Mater Med 19:703–711.
19. Ahsan T, Sah RL. 1999. Biomechanics of integrative cartilage repair. Osteoarthritis Cartilage 7:29–40.
20. Salem SA, Al-Hassani ST, Johnson W. 1975. Aspects of the mechanics of driving nails into wood. Int J Mech Sci 17: 211–225.
21. Pallante AL, Bae WC, Chen AC, et al. 2009. Chondrocyte viability is higher after prolonged storage at 37 degrees C than at 4 degrees C for osteochondral grafts. Am J Sports Med 37:24S–32S.
22. Chang DG, Iverson EP, Schinagl RM, et al. 1997. Quantitation and localization of cartilage degeneration following the induction of osteoarthritis in the rabbit knee. Osteoarthritis Cartilage 5:357–372.
23. Hurtig M, Buschmann MD, Fortier L, et al. 2011. Preclinical studies for cartilage repair: recommendations from the International Cartilage Repair Society. Cartilage 2: 137–152.
24. Chu CR, Szczodry M, Bruno S. 2010. Animal models for cartilage regeneration and repair. Tissue Eng Part B Rev 16:105–115.
25. Schinagl RM, Gurskis D, Chen AC, et al. 1997. Depth-dependent confined compression modulus of full-thickness bovine articular cartilage. J Orthop Res 15:499–506.
26. Korhonen RK, Laasanen MS, Toyras J, et al. 2002. Comparison of the equilibrium response of articular cartilage in unconfined compression, confined compression and indentation. J Biomech 35:903–909.
27. Armstrong CG, Lai WM, Mow VC. 1984. An analysis of the unconfined compression of articular cartilage. J Biomech Eng 106:165–173.
28. Han E, Chen SS, Klisch SM, et al. 2011. Contribution of proteoglycan osmotic swelling pressure to the compressive properties of articular cartilage. Biophys J 101:916–924.
29. Shepherd DET, Seedhom BB. 1999. The "instantaneous" compressive modulus of human articular cartilage in joints of the lower limb. Rheumatology (Oxford) 38: 124–132.
30. Rho JY, Ashman RB, Turner CH. 1993. Young's modulus of trabecular and cortical bone material: ultrasonic and microtensile measurements. J Biomech 26:111–119.
31. Choi K, Kuhn JL, Ciarelli MJ, et al. 1990. The elastic moduli of human subchondral, trabecular, and cortical bone tissue

and the size-dependency of cortical bone modulus. J Biomech 23:1103–1113.
32. Bugbee W, Cavallo M, Giannini S. 2012. Osteochondral allograft transplantation in the knee. J Knee Surg 25:109–116.
33. Mall NA, Harris JD, Cole BJ. 2015. Clinical evaluation and preoperative planning of articular cartilage lesions of the knee. J Am Acad Orthop Surg 23:633–640.
34. Su AW, Chen Y, Dong Y, et al. 2014. Energy density and shear are mechanical mediators of cartilage damage during impact. Trans Orthop Res Soc 39:1076.
35. Claes L, Augat P, Suger G, et al. 1997. Influence of size and stability of the osteotomy gap on the success of fracture healing. J Orthop Res 15:577–584.
36. Duchow J, Hess T, Kohn D. 2000. Primary stability of press-fit-implanted osteochondral grafts. Am J Sports Med 28:24–27.

SUPPORTING INFORMATION

Additional supporting information may be found in the online version of this article at the publisher's web-site.